



Optionally Reinforced Columns Under Simulated Seismic and Time Varying Axial Loads: Advanced HYLSE-2 Testing

Jelena Ristic¹, Zijadin Guri^{2*}, Danilo Ristic³

¹ Department of Civil Engineering, Faculty of Engineering, International Balkan University (IBU), 1000 Skopje, Republic of North Macedonia.

² Faculty of Civil Engineering, University of Pristina, Pristina, Kosovo.

³ Institute of Earthquake Engineering and Engineering Seismology (IZIIS), Skopje, SS Cyril and Methodius University in Skopje, 1000 Skopje, Republic of North Macedonia.

Received 05 July 2024; Revised 21 September 2024; Accepted 28 September 2024; Published 01 October 2024

Abstract

Steel- and composite-reinforced columns (SRC and CRC columns) provide alternative solutions for common and harsh environments. Although extensive research has been conducted on these columns, direct comparative studies of SRC and CRC columns under seismic conditions, with consistent testing and realistic load simulations, remain limited. This study examined the nonlinear seismic responses of nine ordinary steel-reinforced concrete column models constructed alternatively with normal-strength and high-strength concretes under simulated earthquakes and time-varying axial loads. A developed advanced HYLSE-2 seismic testing system was employed to conduct seismic tests. Spiral transversal reinforcement with pitches of 6.0 and 9.0 cm was used to explore the effects of concrete confinement. The HYLSE-2 seismic tests, conducted under various interactively simulated earthquake intensities and time-varying axial loads, yielded crucial experimental results. Additionally, an extensive complementary analytical study was conducted to provide comparative insights between steel-reinforced columns (SRC) and composite-reinforced columns (CRC) with novel glass fiber-reinforced (GFRP) bars. The analytical study was conducted using experimentally proven advanced nonlinear analytical micromodels. The analytical results highlight the hysteretic behavior of columns reinforced with ordinary steel and novel GFRP reinforcing bars under the simulated combined effects of reversed cyclic bending and time-varying axial loads. The findings form a critical basis for advancing seismic design strategies for SRC and CRC columns exposed to strong earthquakes and high-time variations in axial loads.

Keywords: Concrete; Columns; Steel Bars; Glass Fiber-Reinforced Plastic (GFRP); Testing; Earthquakes; Nonlinear Response.

1. Introduction

The seismic safety of structures is largely determined by the actual seismic performance of reinforced concrete (RC) columns. The design of columns with advanced seismic performance is a critical safety issue. Ordinary steel bars are traditionally used as reinforcements in the construction of RC columns. Recently, numerous studies have been conducted to introduce fiber-reinforced plastic (FRP) bars as a novel reinforcing solution to prevent corrosion in aggressive environments. Innovative studies have attracted increasing attention for the suitable design of steel- and FRP-reinforced columns exposed to strong seismic loads.

Columns are primarily exposed to the combined action of seismically induced bending and time-varying axial loading owing to the adopted specific structural characteristics or direct action of earthquake excitations [1]. Studies on

* Corresponding author: zijadin.guri@uni-pr.edu

<http://dx.doi.org/10.28991/CEJ-2024-010-10-09>



© 2024 by the authors. Licensee C.E.J, Tehran, Iran. This article is an open access article distributed under the terms and conditions of the Creative Commons Attribution (CC-BY) license (<http://creativecommons.org/licenses/by/4.0/>).

the bidirectional response of RC columns have shown that bidirectional loading reduces the drift capacity and accelerates strength and stiffness degradation [2-6]. Test results have shown that the axial N load ratio S of the column's cross-section area A_c , ($S = N/\sigma_c A_c$; where σ_c is compressive strength of concrete) significantly affects the displacement capacity [4, 7, 8]. Menegon et al. [9] conducted a study using the drift model formulated in another study [10], demonstrating that for an increased axial load ratio from 0.1 to 0.3, the displacement capacity of the column is reduced by a factor of 2.3. Incorrect design consideration of axial load effects can lead to severe seismic damage or column collapse. Complex and expensive strengthening and repair techniques are generally required for enhancing the strength and ductility of columns, including RC jacketing, steel jacketing, externally bonded FRP, near-surface-mounted FRP, shape-memory alloy jacketing, and hybrid jacketing [11, 12].

Novel fiber-reinforced polymer (FRP) bars have been introduced as alternative reinforcement because of their superior mechanical properties and durability. These FRP elements are particularly suited for reinforced concrete structures exposed to harsh environmental conditions [13]. FRP bars offer several advantages over steel bars, including a higher strength-to-weight ratio, electromagnetic neutrality, high cutting ability, and lightweight and flexible characteristics. Most currently used FRP bars are made of carbon (CFRP), glass (GFRP), or aramid (AFRP) [14, 15]. Numerous studies have been conducted to determine the mechanical properties of GFRP bars, particularly their compressive strengths. The reported compressive strength of GFRP bars is 55–65% of their tensile strength (ACI 440.1R, 2006) [16, 17]. Although the compressive and tensile strengths are affected by the fiber volume, fiber type, resin material, and manufacturing process, the modulus of elasticity is similar for compression and tension [18]. The behavior of columns reinforced with GFRP and steel bars has been studied recently [13, 19, 20].

GFRP-reinforced members subjected to flexure exhibit significantly greater cracking and displacement than elements reinforced with steel bars [21]. The contribution of GFRP bars to the axial capacity of the columns is less than that of steel bars. It has been observed that using FRP reinforcement does not increase the compressive capacity of the columns but delays the buckling of the longitudinal bars [13, 22, 23]. The bending moment and axial load capacities of steel-reinforced columns are higher than those of columns reinforced with GFRP bars, although both exhibit similar ductility [19-21]. The compression modulus of GFRP bars is lower than their tension modulus; hence, numerous studies and design codes [16, 17] do not consider the contribution of GFRP bars as a compressive reinforcement in columns and beams. Recent studies have focused on various structural problems, including the nonlinear behavior of short columns and columns integrated into RC-infilled frame structures [24, 25] or particular joints and connections [26-28]. In response to these problems, various retrofitting methods have been proposed and studied [29, 30].

As can be implied from above, extensive studies have been conducted on columns reinforced with common steel or with novel GFRP bars. However, specifically targeted comparative studies of SRC and CRC columns, using identical testing and analytical micromodels that account for varying concrete strengths and confinements, and successfully simulate the interactive effects of cyclic bending loads and time-varying axial loads have not been sufficiently or comprehensively investigated.

Based on the results of extensive post-earthquake field inspections and available literature, severe and intolerable damage to columns is widely observed owing to the induced complex interactive effects of bending and time-varying axial loads during strong earthquake excitations. Therefore, studies focused on the seismic safety improvement of commonly reinforced columns and innovative GFRP-reinforced columns are crucial. This study builds on the innovative application of our previous advanced experimental results obtained from extensive HYLSE-2 seismic tests conducted under simulated real earthquake conditions. An advanced analytical study was completed based on the developed and extensively used advanced micro modeling concept using unique experimental results. This study's findings present critical original, scientific, and practical benefits.

a) Advanced HYLSE-2 seismic testing system: The developed advanced Hybrid Loading System of Earthquake Responre-2 (HYLSE-2), was implemented to realize extensive experimental study in Japan [31-34]. The pseudo-dynamic HYLSE-2 testing system was employed to test the nonlinear seismic response of the constructed RC column models under the simulated interactive effects of real strong earthquakes and respective time-varying axial loads. The effects of the most critical parameters were experimentally confirmed using the adopted representative testing program, as follows:

- *Achieving new benefits with used results from advanced former experimental tests:* Considering the original results obtained from the former advanced HYLSE-2 experimental tests and the presently available advanced computer analysis software, this study was conducted after many years of preparation.
- *Tested models with ordinary-strength concrete:* Initially, experimental HYLSE-2 seismic tests were performed considering test models constructed with ordinary-strength concrete to obtain basic results.
- *Tested models with high-strength concrete:* Subsequently, a series of HYLSE-2 seismic tests were performed on test models constructed with high-strength concrete to identify existing response effects.
- *Effects of earthquake input intensity:* HYLSE-2 seismic tests were performed at different intensity levels to identify the effects of earthquake intensity on the resulting hysteretic responses of the tested models.

- *Effects of concrete confinement:* HYLSE-2 seismic tests were performed on models constructed with different confinement levels to examine the impact of concrete confinement on actual hysteretic responses.
- *Effects of time-varying axial load on hysteretic response:* HYLSE-2 seismic tests were conducted under simulated time-varying axial loads to evaluate the complex interactive loading effects.

b) Advanced modeling: An advanced and critical analytical study was then conducted to confirm advances in the micro-modeling concept to realistically predict hysteretic responses of similar (tested) optionally reinforced column models with high accuracy.

- *Effects of time-varying axial load on columns reinforced with steel bars:* The effect of time-varying axial load on the tested column reinforced with common steel bars was originally predicted and compared by applying the advanced analytical micro-model.
- *Effects of time-varying axial load on columns reinforced with GFRP bars:* The effect of time-varying axial load on columns reinforced with novel GFRP bars was also successfully predicted and evaluated using the respective refined analytical micromodel.
- *Bending hysteretic response of columns reinforced with steel bars:* The analytical micromodel successfully predicted the bending force-deformation hysteretic response characteristics of columns reinforced with steel bars.
- *Bending hysteretic response of columns reinforced with GFRP bars:* Considering the formulated analytical micromodel, the original characteristics of the bending hysteretic response of columns reinforced with GFRP bars were comparatively computed.

c) Novelty of present research: The severe seismic damage observed in columns during recent earthquakes clearly indicates the need and importance of the present combined experimental and analytical research.

- *Contribution to filling the research gap:* This study was conducted to provide original findings and address existing research gaps. By systematically comparing hysteretic responses, the study provides insights that can enhance seismic design procedures for alternatively reinforced SRC and CRC columns.
- *Integral multitask research flow:* This study comprised a series of interrelated tasks: 1) analyzing HYLSE-2 seismic test results for models with normal-strength concrete; 2) analyzing tests results for models with high-strength concrete; 3) conducting a refined analytical study of the hysteretic behavior of steel-reinforced columns and GFRP-reinforced columns; 4) experimentally validating the developed nonlinear micromodels; and 5) formulating conclusions and recommendations based on the findings.
- *Importance of original research results:* Considering the expected extensive future design of columns alternatively reinforced with common steel and novel GFRP bars in seismic areas, the effects of various controlling variables were evaluated and presented.
- *Advanced steps of applications:* The seismic design of common steel-reinforced columns and columns reinforced with novel GFRP bars in seismic regions can be improved based on the original and comparative research results. Targeted upgrading of the seismic design provisions is also recommended.

Initially, original experimental results were gathered from HYLSE-2 seismic tests on large-scale prototype RC column models subjected to simulated time-varying axial loads. This study presents original comparative findings from advanced analytical evaluations of hysteretic responses in identical and alternatively reinforced column models with ordinary steel and novel GFRP reinforcing bars. Advanced numerical modeling of specimens simulating bending and time-varying axial loads was performed using a refined stress-strain-based modeling concept, experimentally validated through previous research by the authors obtained during their previous related studies [14, 15].

1.1. Study Objectives and Methodology

Columns reinforced with ordinary steel bars have traditionally been used in practice. However, in past earthquakes, heavy damage and collapse of RC columns have been observed owing to inadequate design. The new advanced research was systematically planned and realized [36-40]. Recently, columns reinforced with FRP bars have become a common solution for applications in harsh environments. This study examined the comparative seismic performances of reinforced columns subjected to both simulated earthquake-induced bending and time-varying axial loads. Extensive experimental and analytical research was conducted to qualitatively bridge the existing gaps in research and relevant design options. To realize the complex integrated research objectives, we designed and implemented a specific novel HYLSE-2 seismic testing program and refined numerical modeling.

2. Advanced Hybrid Loading System of Earthquake Response

The hybrid seismic-testing method was first developed in Japan [31-34]. The application and development of this testing method have continued owing to its low cost and capability to provide desirable shaking table features. The inelastic seismic response tests on RC column models under the simulated effects of strong earthquake excitations and

those of time-varying axial loads are part of a wider research project conducted at the Structural Earthquake Engineering Laboratory at Kyoto University, Japan [35]. The seismic tests were conducted by applying the upgraded online computer-controlled hybrid loading system of earthquake response (HYLSER-2), as shown in Figure 1.

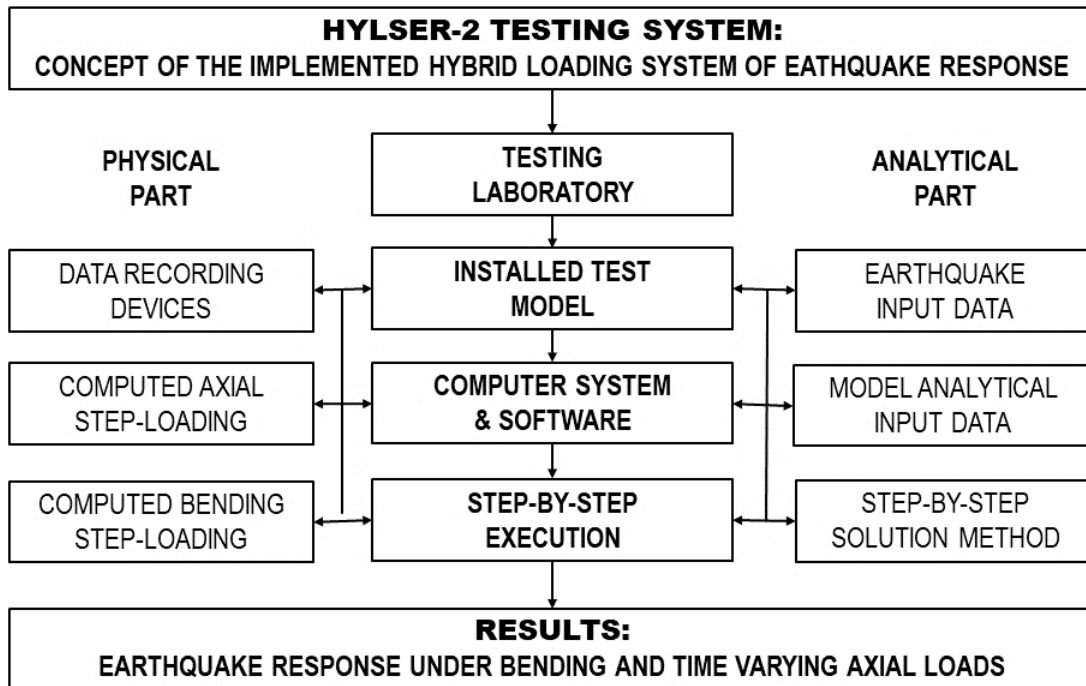


Figure 1. Concept of created hybrid loading system of earthquake response: HYLSER-2

HYLSER-2 testing system contains three integrated parts: (1) **Physical part**: The physical part includes data recording devices, computed increments for the axial step loading, and computed increments for current-step bending loading. (2) **Analytical part**: The analytical part includes numerical earthquake input data, analytical part of model input data including the numerical value of the considered system mass, and system damping of the tested “hybrid-discrete” column system. (3) **Testing laboratory**: The laboratory testing part included the installation of the complete laboratory testing equipment and the construction of the corresponding mechanical support system for adequate assembling of the testing models. In addition, a computer system was provided with specific software to control the test process and the step-by-step execution of the HYLSER-2 semi-dynamic experimental test based on a numerical solution of the respective differential equations of motion. Regarding the considered specific mixed testing concept (with intentionally defined properties of an experimental–analytical testing system), the actual execution time of the HYLSER-2 seismic tests was extended to provide detailed evidence of the damage propagation process.

Figure 2 shows the setup of the column models tested under the simulated earthquake excitation and time-varying axial loads. The experimental model “a” was considered a supported beam with a span divided into three segments of 600 mm each. An initial stiffness of $K_0 = 6500$ kN/m was obtained experimentally. However, the system’s effective mass and damping of 5.0 % were adopted analytically.

HYLSER-2: MODEL SET-UP FOR SEISMIC RESPONSE TESTING SIMULATING BENDING AND VARYING AXIAL LOADS

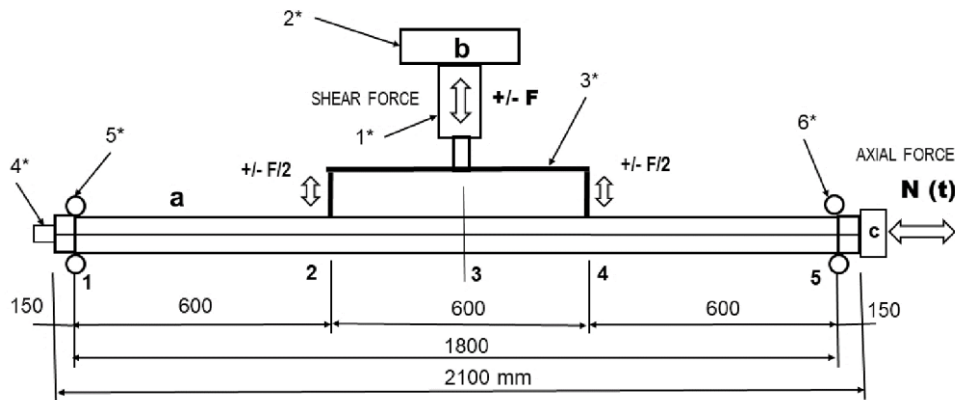


Figure 2. Set-up of column model for seismic response testing under simulated time varying axial load (dimensions in mm)

The three segments were defined by cross-sections denoted by points 1, 2, 4, and 5, respectively. Point 3 indicates the middle span, whereas points 1 and 5 indicate the left and right model supports from the lower side. System “b” was used for the application of the computed current displacement to record the real effective restoring force (+/-F). The bending force was generated using an electro-hydraulic actuator 1* connected to supporting segment 2*. The constructed rigid steel system 3* provided cyclic loading at two loading points: points 2 and 4. A time-varying axial force was applied by installing an unbounded high-strength steel bar 4* into the central, circular pipe-like opening along the model length. The steel bar, installed with highly minimized friction, was fixed to the left end face of the model. However, on the right end, it was fixed to an electro-hydraulic actuator used for the application of the computed current time-varying axial force. The tensile force applied on the steel bar was transformed into a compressive force on the tested model because the hydraulic actuator was directly supported by the right concrete face of the model.

Points 5* and 6* indicate the constructed supports of the model on the upper side activated when an upward bending force was applied. The time-varying axial force, N(t), was calculated for each testing step using (1).

$$N(t) = N_0 + (N_{max} - N_0) p(t) \tag{1}$$

The initial (average) axial force $N_0 = 176.5$ kN and maximum axial force $N_{max} = 265.0$ kN were considered to simulate the realistic testing conditions. Using the measured restoring force F(t) and the known maximum restoring force F_{max} defined with the realized initial static tests, the participation factor p(t) was calculated for each step $p(t) = F(t) / F_{max}$. For the step with recorded $F(t) = +F_{max}$, $p(t) = 1$, the resulting axial force becomes $N_{max} = 265.0$ kN, while for the step with recorded $F(t) = -F_{max}$, $p(t) = -1$, resulting axial force becomes $N_{min} = 88.0$ kN.

The experimental process involved solving the related second-order nonlinear differential equation of motion step by step, with the restoring force F measured directly from the actuator. The computed displacement increment in the next step was employed to calculate the total displacement applied by the electrohydraulic actuator. The created experimental testing system HYLSEr-2 enabled the successful realization of advanced seismic response tests for all constructed RC column models with simulated time-varying axial loads.

3. Seismic Tests of RC Column Models Under Simulated Time Varying Axial Loads

3.1. Characteristics of the Tested RC Column Models

The experimental RC column models were constructed considering an identical square cross-section of 150 / 150 mm, identical length of 2100 mm, and identical span of 1800 mm. The models were constructed using two different concretes with the same longitudinal reinforcement.

The longitudinal reinforcement comprised four bars ϕ of 13 mm with a modulus of elasticity $E_s = 210$ GPa and stress at the yield point $f_y = 400$ MPa. A central steel bar ϕ of 30 mm, used for the application of the axial force, was made of high-strength steel with a modulus of elasticity of $E_s = 200$ GPa and stress at the yield point $f_s = 950$ MPa. Normal concrete (type-1) with a modulus of elasticity $E_c = 27$ GPa and a compressive strength $f_c = 45$ MPa was used (Table 1). Table 2 illustrates the cylinder strengths of the high-strength concrete (type-2).

Table 1. HYLSEr-2 seismic tests of constructed column models with normal concrete: Recorded response parameters during tests with simulated El-Centro earthquake and time-varying axial load (* See Section 5.5)

Test	C-Type & EQI (r)	Cylinder f_{ck} (MPa)	Pitch e (cm)	Axial N (kN)	max F +/- (kN)	+/-DM (cm)	+/-FM (kN)	+/-D2 (cm)	+/-F2 (kN)	
1	D4	Normal/r=2.0	46.3	6	Varying	90.0	1.4	85.0	2.0	90.0
						-60.0	-1.1	-52.0	-2.0	-53.0
2	D5	Normal/r=1.3	50.1	6	Varying	94.0	1.4	94.0	2.0	92.0
						-60.0	-1.0	-46.0	-2.0	-56.0
3	D9	Normal/r=2.0	50.5	9	Varying	95.0	1.2	82.0	2.0	90.0
						-62.0	-1.0	-55.0	-2.0	-60.0
4	D10	Normal/r=1.3	43.0	9	Varying	90.0	1.6	88.0	2.0	89.0
						-60.0	-1.1	-55.0	-2.0	-60.0
5	D17	Normal/r=2.0	43.1	9	Varying	90.0	1.3	80.0	2.0	90.0
						-60.0	-1.0	-54.0	-2.0	-55.0
Average for e = 6 cm		52.30	6	Varying	93.00	1.40	89.50	2.0	90.67	
					60.67	-1.05	-49.00	2.0	56.33	
Average for e = 9 cm		43.05	9	Varying	90.00	1.36	83.30	2.0	89.05	
					60.00	-1.03	-54.66	2.0	57.50	
Average for e= 6 & 9 cm		48.60	6 & 9	Varying	91.80	1.38	85.80	2.0	90.20	
					60.40	-1.04	-52.40	2.0	56.80	
* Analytically predicted				A	Varying	86.00	1.00	80.00	2.0	69.00
						65.00	-1.00	-65.00	2.0	60.00

Table 2. HYLSEK-2 seismic tests of constructed column models with high-strength concrete: Recorded response parameters during tests with simulated El-Centro earthquake and time-varying axial load

Test	C-Type & EQI (r)	Cylinder f_{ck} (MPa)	Pitch e (cm)	Axial N (kN)	max F +/- (kN)	+/-DM (cm)	+/-FM (kN)	+/-D2 (cm)	+/-F2 (kN)
11 D11	HS/r=2.0	77.2	6	Varying	102.0	1.0	84.0	2.0	92.0
					-70.0	-1.0	-56.0	-2.0	-60.0
12 D12	HS/r=1.3	67.7	6	Varying	100.0	1.0	85.0	2.0	98.0
					-60.0	-1.0	-55.0	-2.0	-60.0
13 D13	HS/r=2.0	65.4	9/Collapsed	Varying	99.0	1.0	82.0	2.0	92.0
					-65.0	-1.0	-56.0	-2.0	-60.0
14 D14	HS/r=1.3	77.2	9	Varying	99.0	1.2	86.0	2.0	99.0
					-60.0	-1.0	-56.0	-2.0	-60.0
Average P6		69.95	6	Varying	101.00	1.00	84.50	2.0	95.00
					65.00	-1.00	-55.50	2.0	60.00
Average P9		71.30	9	Varying	99.00	1.10	84.00	2.0	95.50
					62.50	-1.00	-56.00	2.0	60.00
Average-G		70.62	G	Varying	100.00	1.05	84.25	2.0	95.25
					63.5	-1.00	-55.75	2.0	60.00

A transverse reinforcement was formed from ϕ five spiral steel bars with pitches $e = 6$ cm and $e = 9$ cm to study the effect of confinement. Three different intensities were considered using the defined earthquake intensity factor r to study the earthquake intensity effect.

The earthquake was characterized by a starting intensity factor $r = 1.0$, representing the El Centro earthquake, which was used to drive the model's response up to the yielding point. Subsequently, the defined basic intensity "yielding earthquake" was increased by 30% and 100%, by considering earthquake intensity factors $r = 1.3$ and $r = 2.0$, respectively.

3.2. HYLSEK-2 Seismic Tests of Normal-Strength Concrete Models with Simulated Time-Varying Axial Load

Five seismic tests were conducted on steel-reinforced normal-strength concrete models under the simulated effects of time-varying axial loads using the HYLSEK-2 testing system. Table 1 illustrates the design parameters of the tested models and representative results. For the five pseudo-dynamic tests, D4, D5, D9, D10, and D17, the earthquake intensity factors were $r = 2.0$, $r = 1.3$, $r = 2.0$, $r = 1.3$, and $r = 2.0$, respectively. For models D4 and D5, the spiral reinforcement was arranged with a pitch of 6.0 cm.

However, for models D9, D10, and D17, a pitch of 9.0 cm was used. Considering the time-varying axial loads, the hysteretic responses exhibited strong asymmetrical shapes. The different restoring forces obtained on both sides represent the most critical parameters investigated and evaluated in this study. Considering different levels of earthquake intensity and confinement, differences in the recorded shapes of the hysteretic seismic responses were identified.

Table 1 illustrates the selected parameters characterizing the hysteretic seismic response as follows: (1) recorded max F (+/-) - maximum positive and negative restoring forces; (2) DM (+/-) and FM (+/-) - positive and negative deformations and restoring forces for identified "yielding point" and (3) D2 (+/-) and F2 (+/-) - for the set deformation $D2 = +/- 2.0$ cm, the recorded positive and negative restoring force at the "hysteretic response contours" (HR-contours). The lower three rows of Table 1 illustrate the average values for the tested models with $e = 6.0$ cm and with $e = 9.0$ cm and the common mean values for all tested models. In the lowest row of Table 1, the analytically predicted (marked with *) comparative values considering a pitch of $e = 6.0$ cm (see Section 5.5) are shown. The experimental and analytical results show a high level of correlation, confirming the correctness of the HYLSEK-2 testing system and the formulated refined nonlinear analytical model. For example, if we consider the case of the experimentally recorded positive max F = 91.8 kN and analytically predicted positive maxF = 86.0 kN, a difference of only 6.7 % exists. The maximum negative values were experimentally recorded and analytically computed. For restoring forces max F(-) = -60.4 kN and max F(-) = -65 kN, the obtained difference of approximately 7.6 % remained within acceptable and expected ranges.

The difference between the maximum restoring forces defined experimentally for the positive and negative sides was significant (51.9%). The "HR-contours" of hysteretic seismic responses were used to comparatively present the

experimental results. The HR contour shows the hysteretic response for each experimental seismic test. Characteristic points M, L, M*, and L* are shown on each HR contour. The four points on the HR-contour represent the “yielding point” and the “point of ultimate deformation response”. Figure 3 shows the representative points on the HR contour obtained for the seismically tested column models D5 and D4 under simulated El Centro earthquakes of different intensities ($r = 1.3, r = 2.0$) and time-varying axial loads. Figure 4 shows the representative points on the HR contours obtained for the seismically tested column models D10 and D9 under the simulated El Centro earthquake of different intensities ($r = 1.3, 2.0$) and the respective simulated time-varying axial loads. These two HR-contours reflect the effects of the concrete type and earthquake intensity on the hysteretic response because the remaining parameters of the models were considered identical. Figures 3 and 4 show that the HYLSEER-2 seismic testing system represents the most successful and inexpensive approach for confirming the effects of critical parameters controlling the seismic safety of the most exposed elements of any integral structural system.

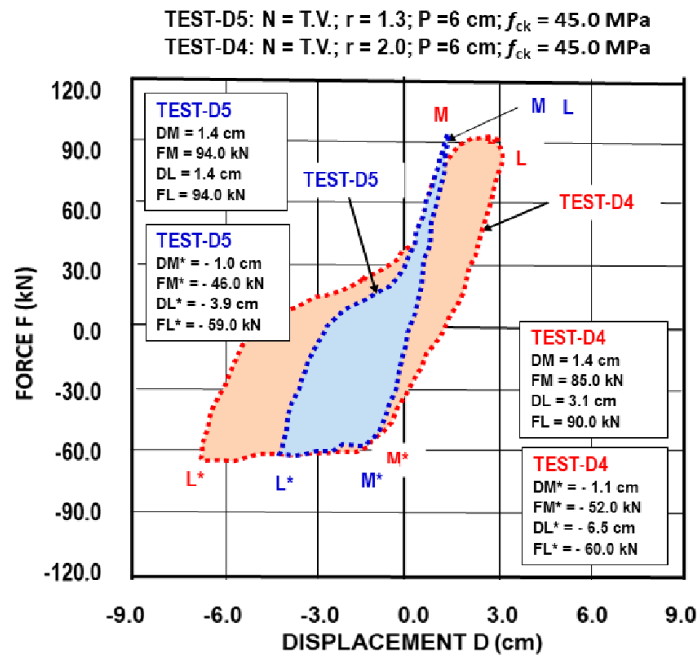


Figure 3. Representative points on recorded final HR-contours from seismically tested column model D4 and D5 under simulated El-Centro earthquake and time varying axial load

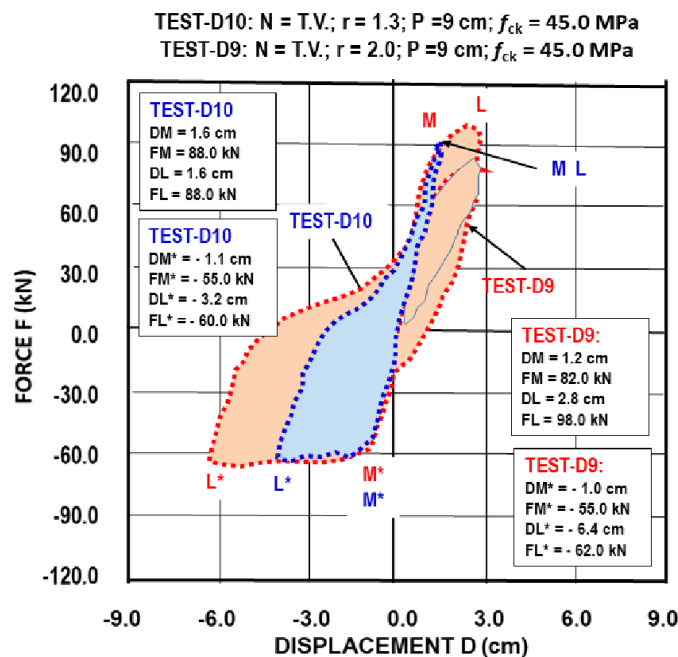


Figure 4. Representative points on recorded final HR-contours from seismically tested column model D9 and D10 under simulated El-Centro earthquake and time-varying axial load

3.3. HYLSEK-2 Seismic Tests of High-Strength Concrete Models with Simulated Time-Varying Axial Loads

Four seismic tests of steel-reinforced high-strength column models were conducted under simulated time-varying axial loads. Table 2 illustrates the parameters related to the tested models and recorded seismic responses.

An earthquake intensity factor of $r = 2.0$ was applied for tests D11 and D13. For tests D12 and D14, an earthquake intensity factor of $r = 1.3$ was used. The transverse spiral reinforcements of models D11 and D12 were used with a pitch of 6.0 cm. However, for models D13 and D14, a pitch of 9.0 cm was used. Table 2 illustrates the experimentally defined parameters controlling the seismic responses of the four tested high-strength concrete models. The following three rows of Table 2 contain the average values for the models with pitch $e = 6.0$ cm, $e = 9.0$ cm, and the common mean values for all four tested models.

The difference between the maximum restoring forces defined experimentally for the positive and negative sides was significant (57.4%). Representative HR contours were considered for the tests of the high-strength concrete models under the simulated effects of time-varying axial loads.

Analogously, on each “HR-contour” presented are points M, L, M*, and L* that control the shapes of the recorded seismic responses. Figure 5 shows the stable hysteretic responses obtained for the seismically tested models D12 and D11 under the simulated El Centro earthquake with defined intensities $r = 1.3$ and $r = 2.0$, respectively.

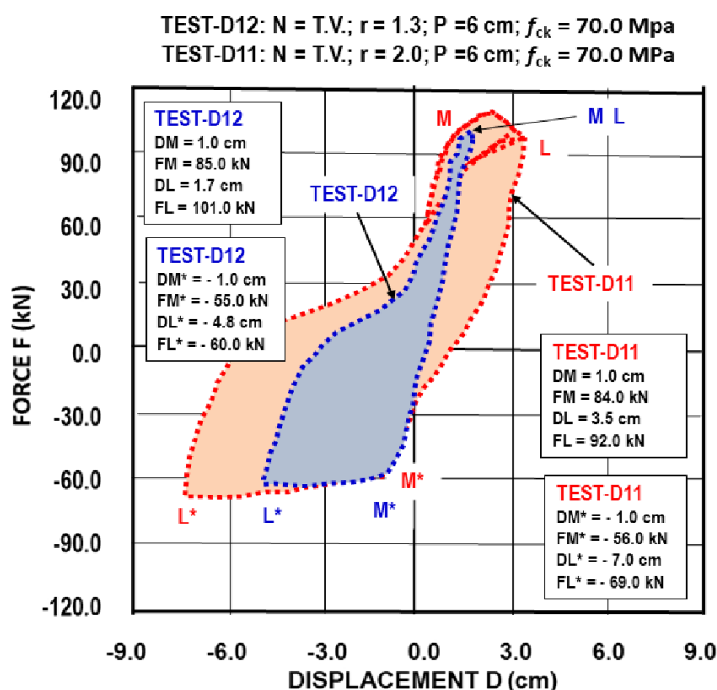


Figure 5. Representative points on recorded final HR-contours from seismically tested column model D11 and D12 under simulated El-Centro earthquake and time-varying axial loads

For the tested models D12 and D11, the obtained “HR-contours” are wide and exhibit different nonlinear behavior owing to the simulated different earthquake intensity represented by $r = 1.3$ and $r = 2.0$. In both cases, the seismic response was stable and without collapse, owing to the improved confinement with the smaller pitch of the spiral reinforcement $e = 6.0$ cm.

Figure 6 shows the representative points on the HR contours for the seismically tested column models D14 and D13, adopting (as above) identical earthquake input intensity factors $r = 1.3$ and $r = 2.0$, respectively. For experimental model D14, a stable hysteretic response was obtained. However, experimental model D13 experienced a total collapse.

The significant difference in models D14 and D13 seismic responses was attributable to directly resulted from the different earthquake intensities. Moreover, a reduced confinement level was implemented for both models with the same pitch $e = 9.0$ cm of spiral transverse reinforcement.

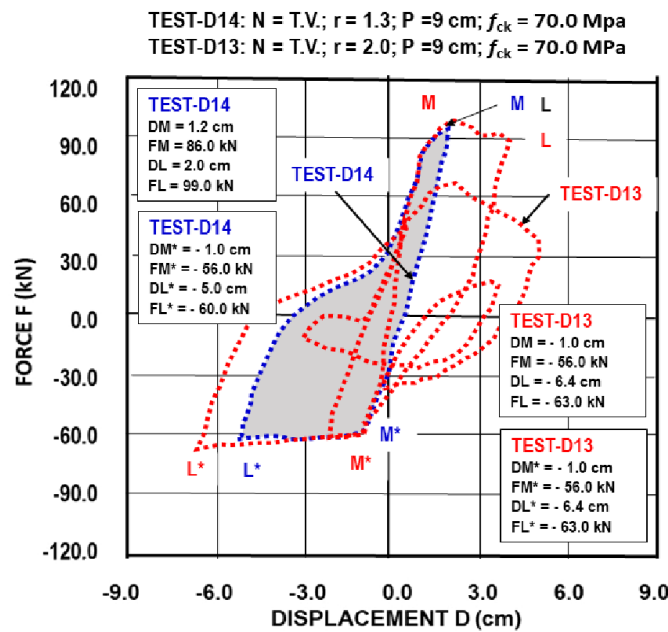


Figure 6. Representative points on recorded final HR-contours from seismically tested column model D13 and D14 under simulated El-Centro earthquake and time-varying axial loads

4. Modeling of Steel and GFRP Columns Under Bending and Time-Varying Axial Loads

The analytical study represents critical complementary research providing extended evidence on the specimen response, which was impossible to define with the HYLSEK-2 seismic tests. An analytical study of the seismic performance of ordinary steel-reinforced and novel GFRP-reinforced column models was conducted by applying the formulated, refined, and experimentally confirmed 3D nonlinear analytical models [14, 15].

4.1. Mechanical Properties of Steel and GFRP Bars

Table 3 illustrates the modeling and loading details of the analytically studied steel and GFRP-reinforced columns. Table 4 illustrates the mechanical properties of the steel reinforcements.

Table 3. Modeling and loading of columns with details of steel and GFRP reinforcement

Model	Reinforcement type	Longitudinal reinforcement	Transversal spiral reinforcement	Loading of models	
				Axial (compressive)	Bending
M3	Steel	4Φ13	Φ5/6 cm	time varying	cyclic
M3A	GFRP	4Φ10	Φ5/6 cm	time varying	cyclic

Table 4. Mechanical properties of steel used reinforcing bars

Diameter [mm]	Material	Tensile elastic modulus E_s [GPa]	Yield strength f_y [MPa]	Ultimate strength [MPa]	Yield strain [%]	Elongation [%]
13	Steel	210	400	560	0.2	5

Table 5 illustrates the mechanical properties of the novel GFRP bars. The correct modeling parameters of the stress-strain relationship were adopted from the tests presented in our previous study [14, 15].

Table 5. Mechanical properties of used GFRP reinforcing bars

Diameter [mm]	Material	Tensile elastic modulus [GPa]	Tensile strength [MPa]	Ultimate strain in tension [%]
10	GFRP	50	1100	2.5

4.2. Refined Finite Element Analysis Model

Considering the identical geometry of the analytical and tested models, the refined finite element analysis (FEA) study focused on modeling two types of specimens: (1) a column model reinforced with equal ordinary steel reinforcing

bars and (2) a column model reinforced with composite GFRP reinforcing bars, simulating the same loading protocol up to deep nonlinearity. The adopted earthquake-like loading protocol and the simultaneous axial action of time-varying cyclic shear loading made the analytical study complex. A fiber section modeling technique was implemented using SeismoStruct software to capture the complex response phenomena [40]. The column specimen was modeled with four 3D nonlinear fiber-based finite elements spaced between five nodal points. Five additional integration sections per element were considered to capture the curvature distribution along each finite element realistically. The considered cross sections were discretized into a refined fiber mesh considering specific fibers for the confined concrete, unconfined concrete, actual steel, and GFRP reinforcing fibers.

4.3. Stress–Strain Modeling of Concrete and Reinforcing Bars

Chang and Mander's model (1994) [41] was chosen to model the nonlinear behavior of the concrete, using a mean compressive strength of 48.0 MPa, a mean tensile strength of 4.8 MPa, a modulus of elasticity of 32 562.5 MPa, and a strain at peak stress of 0.002. Non-dimensional critical compressive and tensile strain coefficients were used to determine the resulting form and shape of the hysteretic curve. The well-known Menegotto-Pinto steel model [36], with a modulus of elasticity of 2×10^5 MPa and a yield strength of 575.0 MPa, was used to model the nonlinear behavior of the steel reinforcement. Finally, the behavior of the GFRP reinforcement bars was represented using a linear model with a modulus of elasticity of 5×10^4 MPa, tensile strength of 1.1×10^3 MPa, compressive strength of 7×10^2 MPa, and specific weight of 50 kN/m³.

4.4. Nonlinear Stress–Strain Based Numerical Analysis Strategy

The refined numerical nonlinear stress–strain-based analysis strategy was established by correctly selecting specific controlling parameters. These included the following. (1) With the defined total number of solution steps $N_s = 800$ and the selected "solution quasi-time step" $dt = 0.005$ s, the "total solution time" was $T = 4.4$ s; (2) the selected successful iterative strategy included: (a) Maximum number of iterations for each solution increment $IT = 40$; (b) maximum number of updates of tangent stiffness matrix for each increment $NSA = 35$; (c) divergence iteration $DI = 35$; (d) maximum tolerance $maxT = 1e20$; (e) maximum step reduction $maxSR = 0.001$; and (f) minimum number of solution iterations $minSI = 1$; and (3) updated correct convergence criteria involving: (3a) mixed displacement/rotation based criterion; with (3b) displacement tolerance of 0.0001 m and (3c) rotation tolerance 0.0001 rad. To realize the analytical study, a maximum of three iterations per step were performed during the computational process.

4.5. Numerical Modeling of Columns with Ordinary Steel Reinforcement

Figure 7 illustrates the earthquake-like loading protocol, including the simulated cyclic bending and time-varying axial loads. Figure 8 shows the analytically predicted hysteretic force–displacement response of column model M3 reinforced with ordinary steel.

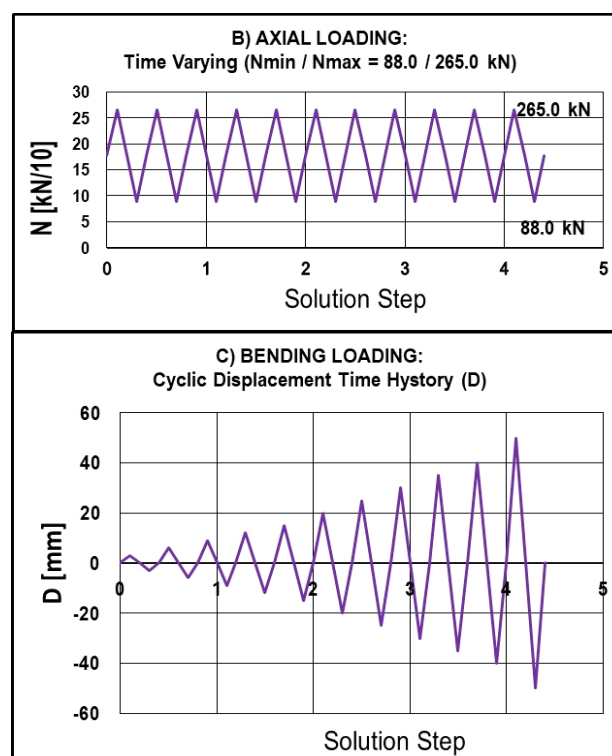


Figure 7. Simulated time varying axial load (up) and cyclic displacement (down)

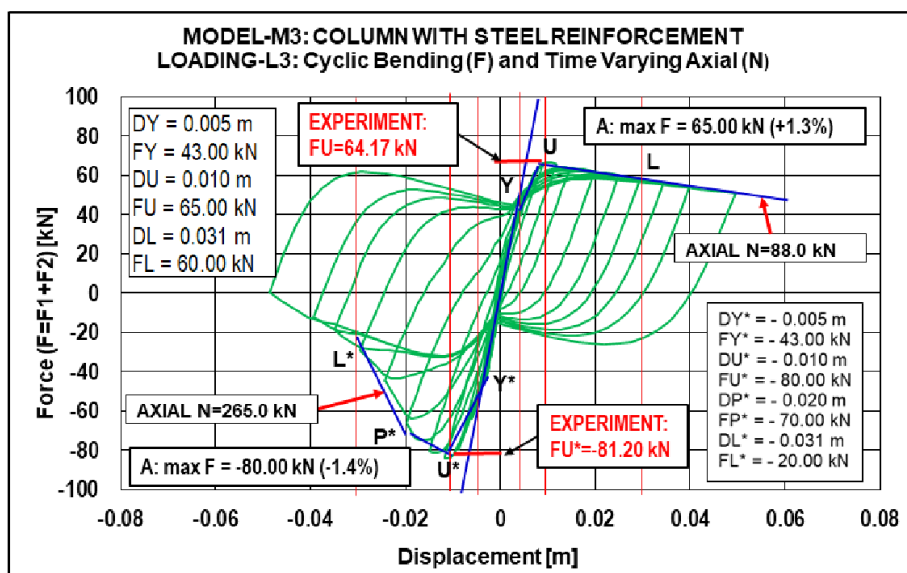


Figure 8. Model M3 with steel reinforcement: Analytically predicted hysteretic force displacement response under simulated cyclic bending and time-varying axial loads

The computed hysteretic relation shows a specific and largely asymmetric shape, directly confirmed by the constructed positive branch of the envelope line defined by the yielding point Y, maximum point U, last common point L, and the asymmetrical negative branch defined by the respective points Y*, U*, P*, and L*. The deciding part of the envelope defined by points U and L is not sharp, showing excellent ductile behavior owing to the simulated effect of the lower axial load on the positive side. The deciding part of the envelope line defined by points U*, P*, and L* became very sharp, indicating poor ductility owing to the simulated effect of the higher axial load on the negative side.

4.6. Numerical Modeling of Columns with Composite GFRP Reinforcement

Figure 7 shows the earthquake-like loading protocol used in this study to derive valuable comparative results. Figure 9 illustrates the hysteretic response obtained from the present analysis of the equivalent column model M3A reinforced with composite GFRP under simulated cyclic bending and time-varying axial loads. Compared with the column reinforced with steel, the computed hysteretic relation is asymmetrical despite being different in shape.

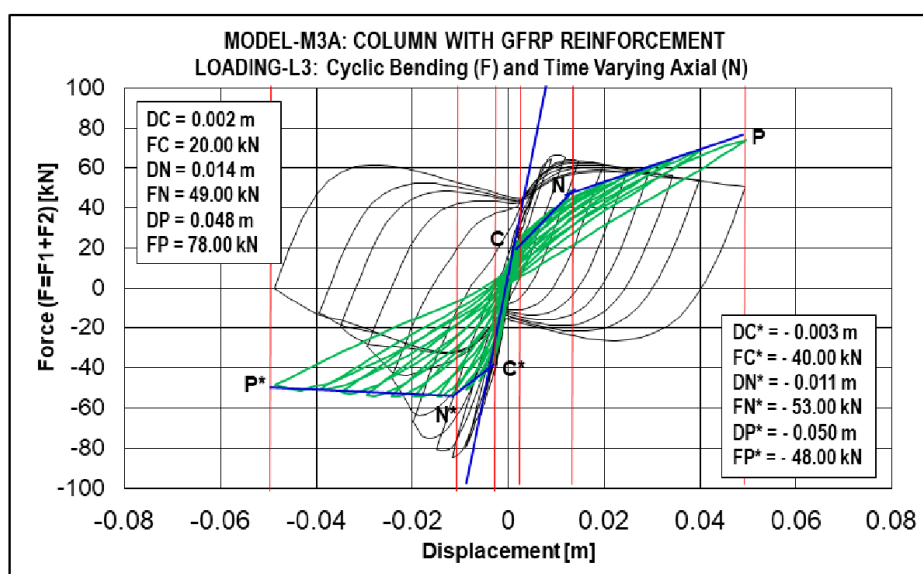


Figure 9. Model M3A with GFRP reinforcement: Analytically predicted hysteretic force displacement response under simulated cyclic bending and time-varying axial loads

The asymmetrical form of the hysteretic response was confirmed by the constructed positive branch of the envelope line defined by the indicated point C, maximum point N, and last common point P, and the related asymmetrical negative envelope branch defined by the respective points C*, N*, and P*. Owing to the simulated effect of the lower axial load on the positive side, the last line segment defined by points N and P exhibits a significant positive slope or positive

stiffness, even for more significant deformations. Owing to the simulated effect of the higher axial load on the negative side, the last line segment defined by points N* and P* showed an insignificant negative slope or negative stiffness but conformed to a ductile response for large deformations. However, the resulting hysteretic response was characterized by a strong pinching effect owing to the combined effects of the linear response of the GFRP bars and the nonlinear stress-strain response of the modeled confined and unconfined concrete fibers.

5. Main Findings from Testing and Numerical Modeling

a) Damage: HYLSE-2 seismic tests with simulated varying axial loads are advantageous owing to their extended test execution time of approximately 45 min. The extended time of the realized HYLSE-2 seismic response tests was used to effectively monitor the crack and damage propagation during the characteristic model response phases. Typical damage was observed in the critical (middle) parts of the tested normal and high-strength concrete column models. The propagation of initial and wider cracks, crushing of concrete, and spilling of concrete were permanently observed at the bottom and upper faces of the deformed specimens. More severe damage was observed in the models constructed with reduced confinement and tested under stronger earthquakes. Similar damage patterns were identified in analytical studies at similar locations.

b) Validated testing and modeling: The original results from the HYLSE-2 seismic tests provided conditions for validating the stress-strain-based numerical modeling strategy. The maximum shear forces obtained from the five HYLSE-2 seismic tests were conducted on normal concrete models with the analytically predicted maximum shear force under simulated cyclic bending and time-varying axial loads (Figure 10). The recorded differences in positive and negative shear forces were insignificant (max 10.4 %). These comparative results confirm the excellent accuracy of the experimental seismic tests and the suitability of the formulated refined nonlinear analytical model. Figure 11 shows the maximum shear forces obtained from the four HYLSE-2 seismic tests conducted on the high-strength concrete models with the calculated average maximum shear force from all four tests under simulated cyclic bending and identical time-varying axial loads. Moreover, it indicates that the recorded differences were insignificant (max 10.0%). This result confirms the consistency of the experimentally defined maximum positive and negative shear forces.

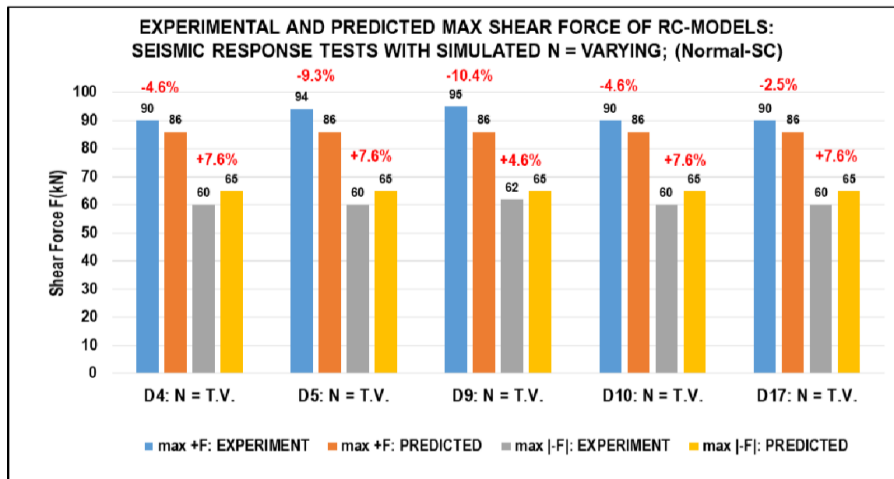


Figure 10. Compared max shear forces (+/-) defined experimentally and predicted analytically (models constructed with application of normal concrete)

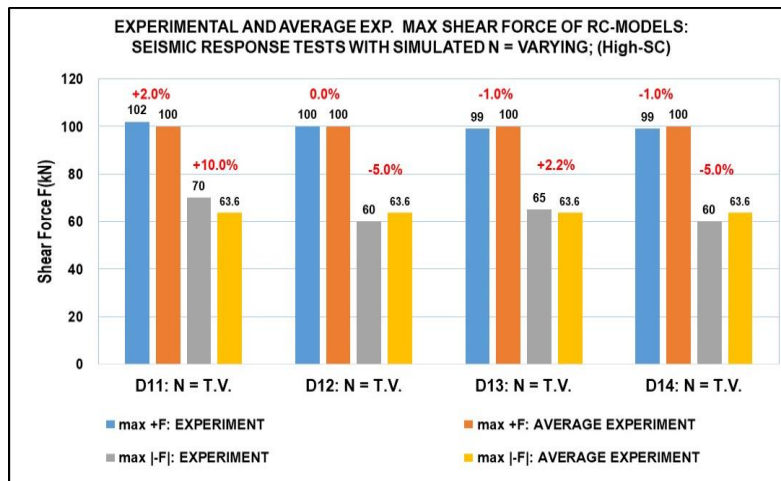


Figure 11. Compared max shear forces (+/-) defined experimentally for single test and defined average experimental from all tests (models constructed with application of high strength concrete)

c) Effects of time-varying axial loads: The shape of the hysteretic response of columns reinforced with steel or GFRP bars was significantly affected by the effective time-varying axial load level. Regarding the column reinforced with steel bars, the obtained results were maximum restoring forces of 65.0 kN and 80.0 kN on the positive and negative sides, respectively, under simulated time-varying axial loads. The resulting difference was statistically significant, 23.1%. The recorded HR contour shows a largely asymmetric shape (Figure 8). For the column reinforced with GFRP bars, respective restoring forces of 40.0 kN and 55.0 kN were recorded under simulated time-varying axial load. A significant difference amounting to 37.5% was also observed. The shape of the recorded HR contour of the GFRP-reinforced column model exhibits was exposed a significant pinching effect (Figure 9).

d) Stiffness and deformability: The difference in stiffness characteristics of columns reinforced with ordinary steel bars or GFRP bars was significant. For columns reinforced with steel bars, the recorded stiffness was considerably larger than the stiffness of the column reinforced with GFRP bars (Figures 8 and 9). The results show that columns reinforced with GFRP bars are generally exposed to significantly larger deformations.

6. Conclusions

Considering the original results obtained from the specifically targeted pseudo-dynamic seismic tests and advanced analytical complementary study, relevant conclusions regarding the seismic design of columns reinforced with ordinary steel bars or novel GFRP bars are derived as follows:

- In this study, a significant difference in concrete strength was found for the respective models (approximately 55.5%). The tested five normal-strength concrete models and four tested high-strength concrete models, having strengths of 45 MPa and 70 MPa, respectively, did not have a significant effect on the column's hysteretic response. This was owing to the prevailing effect in response to the considered equal amount (not different) of longitudinal reinforcement. Reinforcement was controlling failure in bending during responses in both cases.
- Regarding the columns tested under time-varying axial forces, for the bending of the induced model under a simulated minimum compressive axial force (min N deformation state), the effect of different confinement levels on the hysteretic response of the column was negligible. However, regarding the induced model's bending under the simulated maximum compressive axial force (max N deformation state), heavy damage or collapse of the RC columns occurred, particularly for models with lower confinement levels and those subjected to higher earthquake intensity levels.
- For columns reinforced with ordinary steel or GFRP, the different induced (time-varying) levels of axial forces had a significant effect. On the side exposed to smaller simulated axial forces, the hysteretic behavior of the column was stable and generally showed pronounced ductility. However, on the side exposed to higher simulated axial forces, the hysteretic behavior exhibited significantly decreased ductility, followed by a rapid decrease in the restoring force, heavy damage, and total failure, particularly regarding lower confinement and higher earthquake intensities.
- Experimental and analytical investigations confirmed that critical behavior or total collapse of steel and GFRP-reinforced columns occurs if their confinement level is poor and the columns are exposed to high levels of varying axial forces generated mainly by earthquakes with higher intensities.
- This study demonstrates that steel-reinforced columns exposed to time-varying axial loads possess significantly higher energy absorption capacities. The original study results confirmed that GFRP-reinforced columns exhibited a significantly smaller energy-dissipation capacity under simulated time-varying axial forces, owing to the observed significant pinching effect in the recorded hysteretic seismic response.
- In the future design of steel-reinforced columns in seismic areas, the potential levels of time-varying axial forces must be reliably estimated and obligatorily considered.
- Regarding the future design of columns reinforced with novel GFRP bars in seismic areas, the ranges of time-varying axial forces and the actual effects of the increased deformability of GFRP columns under seismic loads must be systematically evaluated and considered in the design process.

7. Declarations

7.1. Author Contributions

Conceptualization, D.R.; methodology, D.R., J.R., and Z.G.; software, Z.G. and J.R.; validation, D.R. and Z.G.; formal analysis, Z.G. and J.R.; investigation, J.R., Z.G., and D.R.; resources, D.R.; data curation, J.R. and Z.G.; writing—original draft preparation, D.R.; writing—review and editing, J.R.; visualization, Z.G. and J.R.; supervision, J.R. and Z.G.; project administration, D.R.; funding acquisition, D.R. All authors have read and agreed to the published version of the manuscript.

7.2. Data Availability Statement

The data presented in this study are available upon request from the corresponding author.

7.3. Funding

The authors received no financial support for the research, authorship, and/or publication of this article.

7.4. Acknowledgements

Seismic HYLSEER-2 tests were conducted at the Structural Earthquake Engineering Laboratory of Kyoto University, Japan. GFRP-related tests and complementary analytical research were performed at the RESIN Laboratory, Skopje, representing the regional seismic innovation research center, established by Prof. D. Ristic, PPD, as a long-term benefit from the innovative NATO Science for Peace and Security Project: Seismic Upgrading of Bridges in South-East Europe by Innovative Technologies (SFP: 983828). The authors express their sincere thanks to both laboratories for their valuable support.

7.5. Conflicts of Interest

The authors declare no conflict of interest.

8. References

- [1] Raza, S., Menegon, S. J., Tsang, H. H., & Wilson, J. L. (2022). Axial Load Variation of Columns in Symmetrical RC Buildings Subject to Bidirectional Lateral Actions in Regions of Low to Moderate Seismicity. *Journal of Earthquake Engineering*, 26(5), 2701–2729. doi:10.1080/13632469.2020.1772151.
- [2] Di Ludovico, M., Verderame, G. M., Prota, A., Manfredi, G., & Cosenza, E. (2013). Experimental Behavior of Nonconforming RC Columns with Plain Bars under Constant Axial Load and Biaxial Bending. *Journal of Structural Engineering*, 139(6), 897–914. doi:10.1061/(asce)st.1943-541x.0000703.
- [3] Qiu, F., Li, W., Pan, P., & Qian, J. (2002). Experimental tests on reinforced concrete columns under biaxial quasi-static loading. *Engineering Structures*, 24(4), 419–428. doi:10.1016/S0141-0296(01)00108-0.
- [4] Raza, S., Menegon, S. J., Tsang, H. H., & Wilson, J. L. (2020). Force-displacement behavior of limited ductile high-strength RC columns under bidirectional earthquake actions. *Engineering Structures*, 208, 110278. doi:10.1016/j.engstruct.2020.110278.
- [5] Rodrigues, H., Arêde, A., Varum, H., & Costa, A. G. (2013). Experimental evaluation of rectangular reinforced concrete column behaviour under biaxial cyclic loading. *Earthquake Engineering and Structural Dynamics*, 42(2), 239–259. doi:10.1002/eqe.2205.
- [6] Rodrigues, H., Varum, H., Arêde, A., & Costa, A. (2012). A comparative analysis of energy dissipation and equivalent viscous damping of RC columns subjected to uniaxial and biaxial loading. *Engineering Structures*, 35, 149–164. doi:10.1016/j.engstruct.2011.11.014.
- [7] Raza, S., Tsang, H. H., & Wilson, J. L. (2018). Unified models for post-peak failure drifts of normal- and high-strength RC columns. *Magazine of Concrete Research*, 70(21), 1081–1101. doi:10.1680/jmacr.17.00375.
- [8] Raza, S., Menegon, S. J., Tsang, H.-H., & Wilson, J. L. (2020). Collapse Performance of Limited Ductile High-Strength RC Columns under Unidirectional Cyclic Actions. *Journal of Structural Engineering*, 146(10), 1943–541 0002772. doi:10.1061/(asce)st.1943-541x.0002772.
- [9] Menegon, S. J., Wilson, J. L., Lam, N. T. K., & McBean, P. (2018). RC walls in Australia: seismic design and detailing to AS 1170.4 and AS 3600. *Australian Journal of Structural Engineering*, 19(1), 67–84. doi:10.1080/13287982.2017.1410309.
- [10] Wilson, J. L., Wibowo, A., Lam, N. T. K., & Gad, E. F. (2015). Drift behaviour of lightly reinforced concrete columns and structural walls for seismic design applications. *Australian Journal of Structural Engineering*, 16(1), 62–74. doi:10.7158/S14-002.2015.16.1.
- [11] He, R., Yang, Y., & Sneed, L. H. (2015). Seismic Repair of Reinforced Concrete Bridge Columns: Review of Research Findings. *Journal of Bridge Engineering*, 20(12), 4015015. doi:10.1061/(asce)be.1943-5592.0000760.
- [12] Raza, S., Khan, M. K. I., Menegon, S. J., Tsang, H. H., & Wilson, J. L. (2019). Strengthening and repair of reinforced concrete columns by jacking: State-of-the-art review. *Sustainability (Switzerland)*, 11(11), 3208. doi:10.3390/su11113208.
- [13] De Luca, A., Matta, F., & Nanni, A. (2009). Behavior of full-scale concrete columns internally reinforced with glass FRP bars under pure axial load. *Composites & Polycon*, 15-17 January 2009, Tampa, Unites States.
- [14] Guri, Z., Kokalanov, G., Ristic, D. & Ristic, J. (2018). Modeling of Circular Columns with Ordinary and Composite Reinforcement. *Proceedings of International Conference, Earthquake Engineering and Engineering Seismology*, 13-15 June, 2018, Kraljevo, Serbia.

- [15] Guri, Z., & Misini, M. (2021). Experimental and numerical study of circular columns reinforced with steel and glass FRP bars. *Magazine of Concrete Research*, 73(4), 163–173. doi:10.1680/jmacr.19.00003.
- [16] ACI 440.1R-06. (2006). *Guide for the Design and Construction of Structural Concrete Reinforced with FRP Bars*. American Concrete Institute (ACI), Michigan, United States.
- [17] CAN/CSA-S806-02. (2002). *Design and Construction of Building Components with Fibre Reinforced Polymers*. Canadian Standards Association (CSA), Toronto, Canada.
- [18] Deitz, D. H., Harik, I. E., & Gesund, H. (2003). Physical Properties of Glass Fiber Reinforced Polymer Rebars in Compression. *Journal of Composites for Construction*, 7(4), 363–366. doi:10.1061/(asce)1090-0268(2003)7:4(363).
- [19] Tobbi, H., Farghaly, A. S., & Benmokrane, B. (2012). Concrete columns reinforced longitudinally and transversally with glass fiber-reinforced polymer bars. *ACI Structural Journal*, 109(4), 551–558. doi:10.14359/51683874.
- [20] Hadi, M. N. S., Karim, H., & Sheikh, M. N. (2016). Experimental Investigations on Circular Concrete Columns Reinforced with GFRP Bars and Helices under Different Loading Conditions. *Journal of Composites for Construction*, 20(4), 04016009. doi:10.1061/(asce)cc.1943-5614.0000670.
- [21] Nanni, A. (1993). Flexural Behavior and Design of RC Members Using FRP Reinforcement. *Journal of Structural Engineering*, 119(11), 3344–3359. doi:10.1061/(asce)0733-9445(1993)119:11(3344).
- [22] Elchalakani, M., Ma, G., Aslani, F., & Duan, W. (2017). Design of GFRP-reinforced rectangular concrete columns under eccentric axial loading. *Magazine of Concrete Research*, 69(17), 865–877. doi:10.1680/jmacr.16.00437.
- [23] Weber, A. (2006). Advanced reinforcement technology with GFRP Rebar. *Proceedings 2nd International fib Congress*. 5-8 June, 2006, Naples, Italy.
- [24] Alkhatabi, L., Ali, A. H., Mohamed, H. M., & Gouda, A. (2024). Strain Behavior of Short Concrete Columns Reinforced with GFRP Spirals. *Buildings*, 14(7), 2180. doi:10.3390/buildings14072180.
- [25] Zhang, X., Zhou, Y., Liu, X., Zheng, Y., & Qi, Z. (2024). Study on Seismic Performance of RC Frame Structures Considering the Effect of Infilled Walls. *Buildings*, 14(7), 14. doi:10.3390/buildings14071907.
- [26] Xu, Q., Qian, J., Zhang, Y., Tang, L., Man, D., Zhen, X., & Han, T. (2024). Analysis of Progressive Collapse Resistance in Precast Concrete Frame with a Novel Connection Method. *Buildings*, 14(6), 1814. doi:10.3390/buildings14061814.
- [27] Kalogeropoulos, G., Tsonos, A. D., & Iakovidis, P. (2024). Hysteresis Behavior of RC Beam–Column Joints of Existing Substandard RC Structures Subjected to Seismic Loading–Experimental and Analytical Investigation. *Buildings*, 14(6), 1609. doi:10.3390/buildings14061609.
- [28] Handhal, M. M., Abdulghani, A. W., & Al-Haydary, M. M. (2023). Structural Behavior of Steel Reinforced Concrete Joint Under Flexural Loads. *Civil Engineering Journal (Iran)*, 9(3), 714–730. doi:10.28991/CEJ-2023-09-03-015.
- [29] Zhou, Y., Liu, X., Zhang, X., & Guo, X. (2024). Investigation on Seismic Performance of Reinforced Concrete Frame Retrofitted by Carbon Fiber-Reinforced Polymer. *Buildings*, 14(6). doi:10.3390/buildings14061604.
- [30] Hassooni, A. N., & Al-Zaidee, S. R. (2022). Rehabilitation of Composite Column Subjected to Axial Load. *Civil Engineering Journal (Iran)*, 8(3), 595–611. doi:10.28991/CEJ-2022-08-03-013.
- [31] Okada, T., & Seki, M. (1977). A simulation of earthquake response of reinforced concrete buildings. *6th World Conference on Earthquake Engineering*, 10-14 January, 1977, New Delhi, India,
- [32] Takanashi, K., Udagawa, K., & Tanaka, H. (1980). Pseudo-Dynamic Tests on a 2-Story Steel Frame By Computer-Load Test Apparatus Hybrid System. *Proceedings 7th World Conference on Earthquake Engineering*, Istanbul, 8-13 September, Istanbul, Turkey.
- [33] Okada, T., Seki, M., & Park, Y. J. (1980). Simulation of Earthquake Response of Reinforced Concrete Building Frames to Bi-Directional Ground Motion by IIS Computer-Actuator on-Line System. *Proceedings of the 7th World Conference on Earthquake Engineering*, 8-13 September, Istanbul, Turkey.
- [34] Yamada, Y., & Iemura, H. (1982). Hybrid Analysis on Earthquake Response of Deteriorating Hysteretic Structures. *Proceedings of the Sino-American Symposium on Bridge and Structural Engineering*, 13–19 September, 1982, Beijing, China.
- [35] Ristic, D. (1988). Nonlinear behavior and stress-strain based modeling of reinforced concrete structures under earthquake induced bending and varying axial loads. Ph.D. Thesis, School of Civil Engineering, Kyoto University, Kyoto, Japan.
- [36] Pang, L., Han, Z., Xiao, J., Liu, Z., Qu, W., & Dong, S. (2024). Bearing Capacity of Hybrid (Steel and GFRP) Reinforced Columns under Eccentric Loading: Theory and Experiment. *Buildings*, 14(8), 2472. doi:10.3390/buildings14082472.
- [37] Hadhood, A., Gouda, M. G., Agamy, M. H., Mohamed, H. M., & Sherif, A. (2020). Torsion in concrete beams reinforced with GFRP spirals. *Engineering Structures*, 206, 110174. doi:10.1016/j.engstruct.2020.110174.

- [38] Alsuhaibani, E., Alturki, M., Alogla, S. M., Alawad, O., Alkharisi, M. K., Bayoumi, E., & Aldukail, A. (2024). Compressive and Bonding Performance of GFRP-Reinforced Concrete Columns. *Buildings*, 14(4), 1071. doi:10.3390/buildings14041071.
- [39] Guo, R., Zhang, H., Chen, K., Song, Y., Li, H., Ding, L., & Liu, Y. (2024). Seismic Performance Analysis of Concrete Columns Reinforced with Prestressed Wire Ropes Embedded in Polyurethane Cement Composites. *Buildings*, 14(4), 993. doi:10.3390/buildings14040993.
- [40] Rhouma, M. Ben, Maazoun, A., Aminou, A., Belkassam, B., Vandenbruwane, I., Tysmans, T., & Lecompte, D. (2024). Blast Loading of Small-Scale Circular RC Columns Using an Explosive-Driven Shock Tube. *Buildings*, 14(4), 921. doi:10.3390/buildings14040921.
- [41] Chang, G. A., & Mander, J. B. (1994). Seismic Energy Based Fatigue Damage Analysis of Bridge Columns: Part I-Evaluation of Seismic Capacity. Technical Report No. Nceer-94-0006.